remote sensing

MDPI

Article

Comparison of Hemispheric and Regional Sea Ice Extent and Area Trends from NOAA and NASA Passive Microwave-Derived Climate Records

Walter N. Meier *, J. Scott Stewart, Ann Windnagel and Florence M. Fetterer

National Snow and Ice Data Center, Cooperative Institute for Research in Environmental Sciences, University of Colorado, Boulder, CO 80309, USA; scotts@colorado.edu (J.S.S.); ann.windnagel@colorado.edu (A.W.); florence.fetterer@colorado.edu (F.M.F.)

* Correspondence: walt@colorado.edu

Abstract: Three passive microwave-based sea ice products archived at the National Snow and Ice Data Center (NSIDC) are compared: (1) the NASA Team (NT) algorithm product, (2) Bootstrap (BT) algorithm product, and (3) a new version (Version 4) of the NOAA/NSIDC Climate Data Record (CDR) product. Most notable for the CDR Version 4 is the addition of the early passive microwave record, 1979 to 1987. The focus of this study is on long-term trends in monthly extent and area. In addition to hemispheric trends, regional analysis is also carried out, including use of a new Northern Hemisphere regional mask. The results indicate overall good consistency between the products, with all three products showing strong statistically significant negative trends in the Arctic and small borderline significant positive trends in the Antarctic. Regionally, the patterns are similar, except for a notable outlier of the NT area having a steeper trend in the Central Arctic, likely related to increasing surface melt. Other differences are due to varied approaches to quality control, e.g., weather filtering and correction of mixed land-ocean grid cells. Another factor, particularly in regards to NT trends with BT or CDR, is the inter-sensor calibration approach, which yields small discontinuities between the products. These varied approaches yield small differences in trends. In the Arctic, such differences are not critical, but in the Antarctic, where overall trends are near zero and borderline statistically significant, the differences are potentially important in the interpretation of trends.

Keywords: sea ice; remote sensing; passive microwave; Arctic; Antarctic; sea ice extent; sea ice area

Citation: Meier, W.N.; Stewart, J.S.; Windnagel, A.; Fetterer, F.M. Comparison of Hemispheric and Regional Sea Ice Extent and Area Trends from NOAA and NASA Passive Microwave-Derived Climate Records. *Remote Sens.* **2022**, *14*, 619. https://doi.org/10.3390/rs14030619

Academic Editors: Giuseppe Aulicino and Peter Wadhams

Received: 29 December 2021
Accepted: 23 January 2022
Published: 27 January 2022

1. Introduction

Multi-channel passive microwave sensors provide a consistent and near-complete long-term time series of sea ice conditions. These data represent one of the longest satellite-derived climate records and are a key indicator of climate change over the past 40+ years. They show an Arctic where sea ice is in decline [1,2], while the Antarctic Sea ice environment is more complex with small trends and large interannual variability [2,3].

The climate records are established from a series of sensors on various satellite platforms. The NASA Scanning Multichannel Microwave Radiometer (SMMR) on the Nimbus-7 platform operated from 1978 to 1987. This was followed by a series of Special Sensor Microwave Imager (SSMI) and Special Sensor Microwave Imager and Sounder (SSMIS) on U.S. Defense Meteorological Satellite Program (DMSP) satellites that began operating in 1987 and whose operations continue (as of end-2021). Each of the sensors has similar characteristics, including sensor frequencies and resolutions. More recently, the NASA/JAXA Advanced Microwave Scanning Radiometer for the Earth Observing System (AMSR-E) (2002–2011) and the JAXA AMSR2 (2012–present) sensors have operated and employ a larger antenna that provides greater spatial resolution. For greatest consistency, most sea ice concentration climate records still employ the SMMR-SSMI-SSMIS series.

Several empirical algorithms have been developed to derive sea ice concentration from the passive microwave brightness temperatures (T_B), e.g., [4]. While substantial differences occur between products from different algorithms [5–8], trends and variability have been found to be generally consistent [9].

Here, we compare sea ice extent and area time series from three related sea ice concentration products, all archived at the National Snow and Ice Data Center (NSIDC). Each product is based on a different sea ice concentration algorithm. The first is "Sea Ice Concentrations from Nimbus-7 SMMR and DMSP SSM/I-SSMIS Passive Microwave Data, Version 1" [10], based on the NASA Team (NT) algorithm [11]. The NT algorithm is the basis for the NSIDC Sea Ice Index (SII) [12] product that reports daily and monthly total sea ice extent and area. The second is the "Bootstrap Sea Ice Concentrations from Nimbus-7 SMMR and DMSP SSM/I-SSMIS, Version 3" [13], based on the Bootstrap (BT) algorithm [14]. Both products are produced at NASA Goddard and archived within the NASA Snow and Ice Distributed Active Archive Center (DAAC) at NSIDC. Both have been employed to derive long-term trends in hemispheric and regional sea ice extent and area [3,15,16].

The third product is the NOAA/NSIDC Sea Ice Concentration Climate Data Record [17]. This is a more recently developed approach, a combination of the NT and BT algorithms that focuses on meeting climate data record standards for reproducibility and transparency. This product is discussed further below, including a description of changes in the latest version (Version 4), published in 2021. All three products provide gridded sea ice concentration fields on the NSIDC 25 km polar stereographic projection.

The purpose of this manuscript is to present the Version 4 CDR product and compare long-term extent and area trends from the CDR with the NT and BT products over both hemispheric and region scales. We do not include a specific validation here because the CDR is based on the NT and BT products that have been thoroughly validated, e.g., [7,8,18]. Here we focus on assessing the consistency between the products over their long-term time series from 1979 through 2020.

2. Materials and Methods

The three products are assessed primarily in terms of sea ice extent and sea ice area. Sea ice extent is the total area covered by ice above a prescribed concentration threshold, typically 15% (as used by the SII and herein). Sea ice area is the actual surface area covered only by ice—i.e., concentration is included in the calculation. These are common metrics of sea ice surface conditions and are routinely used in climate assessments, e.g., [1,19]. Sea ice extent is more commonly employed for two reasons. First, passive microwave concentrations, and hence the area calculation, are often biased low, particularly during summer because of surface melt [6]; extent, being a threshold binary indicator, is less affected by these biases. Second, the passive microwave sensors do not cover all the way to the poles, resulting in a "pole hole" in the Northern Hemisphere coverage. The size of the pole hole has varied in the different sensors. For consistency, when calculating area, it is necessary to omit the region of the largest of the pole holes, which is poleward of ~81° latitude. All area estimates for the Northern Hemisphere encompass only the region outside of this pole hole limit. For extent calculations, the pole can be assumed to be ice-covered at >15% and thus extent estimates represent the entire Northern Hemisphere ice-covered region.

The NT and BT algorithms are both empirically derived and employ coefficients of pure surface types (100% ice, 100% open water), called tie points, based on clustering of T_B values or combinations thereof. A linear interpolation between the tie points representing these clusters is used to determine sea ice concentration (fractional coverage within a given region, e.g., a grid cell). We do not delve into further detail here but refer to the algorithm and product references [10–14].

The CDR product is a combination of the output from the NT and BT algorithms. Because of the tendency of algorithms to underestimate concentration, the CDR chooses the higher concentration from the NT and BT output for its estimate at each grid cell. For

consistency at the ice edge, the BT 15% concentration is used as the ice-water threshold. The product also includes an indicator of uncertainty based on the spatial standard deviation of concentration from both NT and BT in 3 × 3 neighborhoods around each grid cell. Other quality indicators include a derived melt state (based on a passive microwave T_B threshold [20]).

Further details on the CDR product can be found in the product User Guide [17] and the Algorithm Theoretical Basis Document (ATBD) [21]. Here, we focus on a brief description of the enhancements made within Version 4.

The most notable change in Version 4 is the addition of the SMMR part of the record, which adds the period of November 1978 to August 1987 to the CDR concentration field. In earlier versions, only the SSMI and SSMIS sensors were processed for the CDR. The 1978 to 1987 SMMR period was previously filled in via use of a "Merged Goddard" field, combining the NASA products [10,13] that covered the full SMMR-SSMI-SSMIS time series. However, the NASA products include manual corrections to remove errors and artifacts in the data. These manual corrections are somewhat subjective and are not tracked, which means the products are not fully transparent and reproducible and thus do not meet standard CDR criteria. Version 4 processes SMMR, SSMI, and SSMIS fields within the fully automated CDR processing stream. The CDR uses the NASA gridded SMMR T_B product [22], the same source used in the NASA NT and BT products.

The second substantial change is the addition of spatial and temporal interpolation to fill coverage gaps, which allows the CDR to match or exceed the NASA products in coverage. Spatial interpolation is carried out at the T_B level to fill in scattered grid cells with missing T_B values using bilinear interpolation from at least three of the four directly adjacent grid cells. Larger spatial gaps (e.g., due to missing swaths) are filled by temporally interpolating concentration values from surrounding days. This is similar to the approach used for the BT and NT products. For the CDR, a 5-day window is used to apply a weighted bracketed interpolation from both sides of the day with missing data. The closest date of valid data on either side (before and after) is used, weighted appropriately. If valid values are not available before and after the missing date, then a one-sided (either before or after) temporal fill is carried out for up to three days.

SMMR only operated every other day in the polar regions, yielding bi-daily fields. The temporal interpolation is also applied to each missing day during the SMMR period. The CDR interpolation fills most of these days and provides a daily concentration product during SMMR; this is in contrast to the NASA NT and BT products, which do not provide fields on SMMR's non-operational days. Even with the interpolation, some missing data remains, including periods with no data. These include a well-known gap from early December 1987 to mid-January 1988 when the F-8 SSMI sensor was not operating. Other multi-day gaps occur in the CDR during June 1979, July to August 1984, and April 1986 due to poor quality of SMMR T_B fields. The pole hole is also filled via a simple fill from the average concentration of the circle of surrounding adjacent grid cells for users that wish to have complete coverage. All spatial and temporal interpolation is fully tracked and included in data quality fields included in the product.

Automated quality control features were also enhanced in Version 4. To remove more land-spillover error (due to a mixture of land and ice-free ocean along the coast within a sensor footprint), both the NT and BT spillover filters are applied. Similarly, both NT and BT weather filters are applied. Weather filters are thresholds in brightness temperature channel combinations that aim to remove weather effects due to atmospheric emission and wind roughening of the ocean. Such phenomena can result in a sea ice signature over the open ocean. These filters effectively remove low concentration ice because they set a minimum cut-off for open water. Typically, this is <15% concentration, but weather filtering can remove higher concentrations and thus affect the location of the ice edge and resulting ice extent and area estimates. Applying both NT and BT filters more stringently removes erroneous weather effects but also affects the ice edge because of the tendency to remove low concentration ice. Other enhancements for Version 4 include updated software,

including the use of the Bootstrap Version 3.1 algorithm code [3], and minor updates to ancillary fields included in the product. The changes in Version 4 and a comparison to Version 3 of the CDR are discussed in more detail in [23].

In this study, we focus on monthly sea ice extent and area trends. A common land mask and pole-hole mask is applied to each of the products, and all concentrations are scaled 0 to 100 percent for consistency. Daily extent is calculated by summing the area of all grid cells where concentration is $\geq$15%. Daily area is calculated by summing the area of the grid cells with concentration $\geq$15% multiplied by the fractional concentration within each grid cell. Monthly total extent and area values are calculated by averaging the daily values within the given month. For the SMMR period, only non-interpolated days are used in the calculations for consistency of the CDR with the NT and BT products. A minimum of 20 days (10 days for SMMR) of valid daily values are required to calculate a valid monthly average.

3. Results

As noted above, the focus of this study is the comparison of long-term trends from the three products: CDR, BT, and NT. Comparisons are carried out for monthly hemispheric extent and area, as well as regional extents and areas.

3.1. Example Concentration Comparison

Before detailing the long-term extent and area trends, we first present an example of concentration differences to show the spatial variation of the three products. In the Northern Hemisphere (Figure 1), two clear patterns are evident. First, the CDR and BT estimates are in much closer agreement than CDR and NT. This is not surprising given the formulation of the CDR algorithm, which uses the highest concentration from BT and NT at each grid point. Because BT concentration is generally higher than NT [6,18,24], it is the dominant component of the CDR. The largest differences between CDR and BT concentrations occur primarily very near the ice edge—within a couple grid cells of the ice-water boundary. These differences reflect differences in post-processing quality control measures. Primarily, this reflects the use of both NT and BT weather filters for the CDR; another factor in some cases would be the temporal interpolation approach, which differs between CDR vs. BT and NT. Compared to the CDR–BT difference, the CDR–NT concentration differences are much larger and more widespread. While differences are relatively small in the high Arctic during winter, the region of large differences extends well into the ice pack from the ice edge.

The second pattern is the seasonality between the Northern Hemisphere month of the winter maximum (March) and summer minimum (September). Again, the CDR–BT field shows much smaller differences than CDR–NT. However, the near ice edge region of more noticeable differences is wider in September than in March. This reflects a mixture of late-summer surface melt as well as freeze-up and early ice formation. The September CDR–NT shows large and widespread differences. These are most pronounced nearer to the ice edge, but even in the high Arctic, the September differences are substantially larger than in March.

Finally, comparison of the two years, 1985 and 2020, shows that the patterns of the differences are not noticeably different between the early year (during the SMMR period) and the later year (during SSMIS). This is not surprising given that intercalibration is carried out to provide consistent concentration, extent, and area estimates across the sensors. While clear noticeable differences between years are not evident here, comparison of extent and area, discussed below, do show some small, but noticeable discrepancies through the time series.

Examining the Southern Hemisphere fields (Figure 2) shows generally similar patterns as the Northern Hemisphere. The CDR–BT fields have much smaller differences than the CDR–NT fields, with noticeable CDR–BT differences largely limited to near the ice edge, but somewhat more widespread in summer than in winter. The CDR–NT differences

are much larger, but in contrast to the Northern Hemisphere, there are widespread large differences in winter as well as in summer. As is the case for the Northern Hemisphere, there is not a noticeable change in the differences between 1985 and 2020.

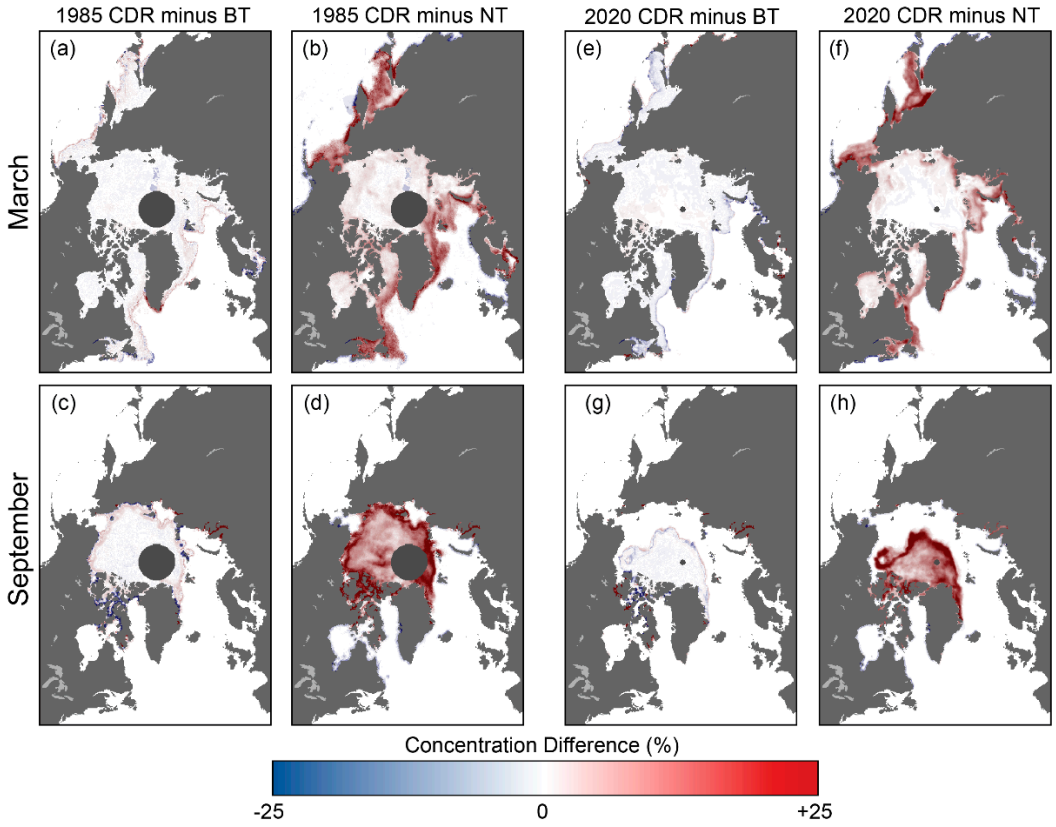

Figure 1. Northern Hemisphere sea ice concentration difference between CDR and the BT and NT algorithm products for March and September for two example years, 1985 (**a**–**d**) and 2020 (**e**–**h**).

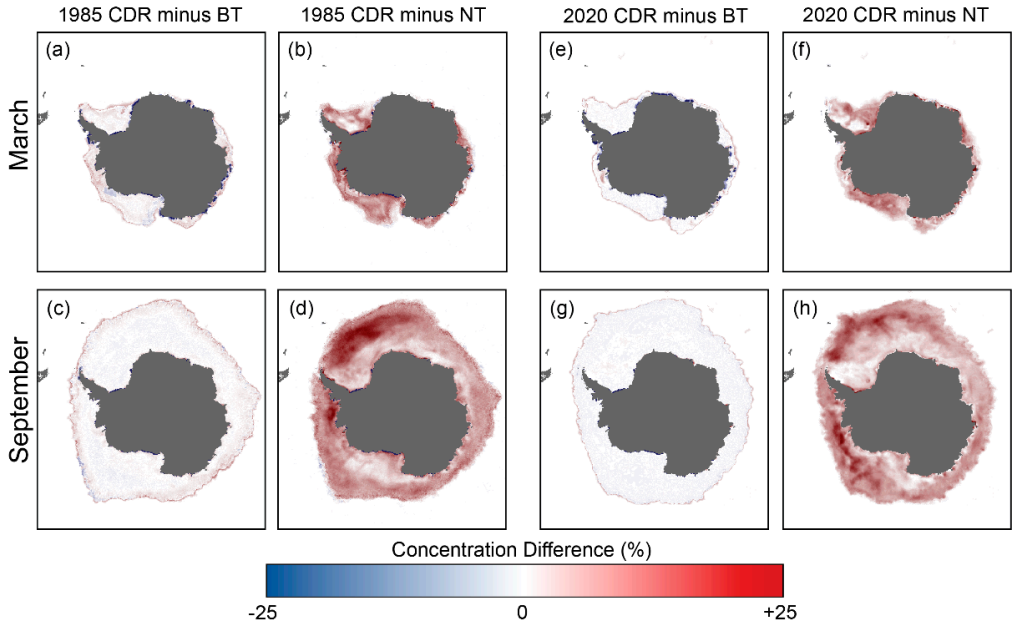

Figure 2. Southern Hemisphere sea ice concentration difference between CDR and the BT and NT algorithm products for March and September for two example years, 1985 (**a**–**d**) and 2020 (**e**–**h**).

3.2. Hemispheric Extent and Area Trends

Next, we examine the hemispheric total extent and area from the three products and their trends over the 1979 to 2020 period. As noted above, extent is the sum of the area of all grid cells above the 15% concentration threshold, while area weights each grid cell by the concentration of the grid cell. Thus, area is more susceptible to biases in concentration, while extent is particularly sensitive near the ice edge where even small differences can result in different classifications between ice-covered and ice-free conditions.

The total extent monthly timeseries from all three products (Figure 3) clearly track the seasonal cycle in the ice cover over the 1979 to 2020 record, with the Southern Hemisphere cycle larger than in the north. All three products appear reasonably consistent for both hemispheres. Interannual variability in the maximum and minimum extents is also noticeable. There is a clear offset between the BT and NT extents, but the extents from BT and CDR are virtually identical (Figure 3a), such that the CDR line is not distinguishable in the figure.

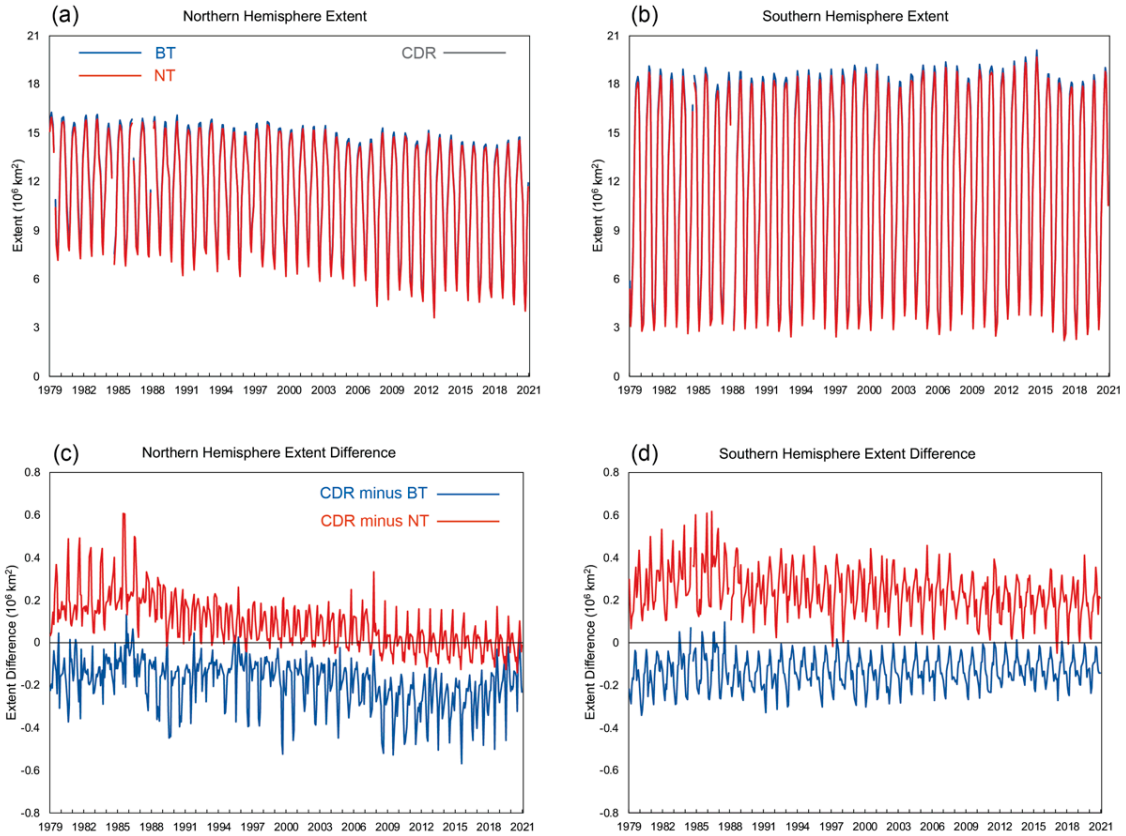

Figure 3. Total monthly sea ice extent, 1979–2020, for (**a**) Northern Hemisphere and (**b**) Southern Hemisphere, and CDR–BT and CDR–NT extent difference for (**c**) Northern Hemisphere and (**d**) Southern Hemisphere.

Only when the extent differences with CDR are plotted (Figure 3c,d), do three products become more easily discriminated. The CDR values are generally larger than NT, but smaller than BT. There is a clear seasonal cycle to the differences. The magnitude of the difference between CDR and BT or NT is largest during summer and smaller during winter. This is likely due to three factors. First, the summer melt causes biases in the products. As noted above, this particularly affects the NT estimates. Though such biases have a smaller effect on extent than on area differences, there could still be some influence near the ice edge when concentrations are very close to the 15% threshold and a bias can tip grid cells from ice-covered to ice-free. Another factor for NT is that the CDR uses only the BT concentration as the ice-edge threshold. In other words, it is the 15% contour in BT

that determines whether a grid cell is ice-covered. Therefore, if NT has a concentration <15%, but BT is >15%, the CDR considers the cell ice-covered (and vice versa for ice-free). Third, there are differences in quality control factors, which influence the BT and CDR ice edge differences, because otherwise they use the same 15% criteria. In particular, the more stringent automated corrections that are applied, including the application of both the BT and NT weather filters and land-spillover corrections, result in a different ice edge between CDR and BT. In general, CDR will tend to remove more ice than BT, resulting in a smaller extent, as seen in Figure 3.

Another notable aspect of the difference timeseries is that there are small but noticeable shifts at points during the record, particularly in the CDR–NT time series. These occur at the SMMR to SSMI transition in August 1987 and in the SSMI to SSMIS transition in January 2008. This reflects differences in the inter-calibration between the sensors. The BT and NT products did their inter-sensor calibration (adjustment of tie points) independently, resulting in slight differences. One additional aspect is that NT adjusted weather filter thresholds between sensors, due to small differences in sensor resolution and frequency [25,26]. Because the CDR relies more on BT (especially for the ice edge discrimination), the CDR inter-calibration aligns better with BT and the differences are smaller, though still present due to the different quality control measures applied.

The differences are more notable (for both BT and NT) during the SMMR part of the record. This reflects poorer quality of the SMMR data overall. For BT and NT, more manual corrections were needed for SMMR than for later data [27]. Because the CDR used only automated measures, larger differences occur for the SMMR period. Note that for SMMR, the monthly average was computed only from the days with actual data not the CDR interpolated missing days of the bi-daily SMMR operation. Therefore, the same days were used in the monthly average for all three products, though there will be some effect due to minor differences in the temporal averaging methodology.

In terms of the overall effects on interpreting the long-term time series, the differences between the products are not consequential in the Northern Hemisphere. All three products show a statistically significant ($p < 0.05$) decline over the full time series, March, and September (and, not shown, other months as well) (Table 1). The differences in the trends between the products are relatively small: ~10% for all months and March, ~10% for CDR–NT for September, and ~1% for CDR–BT for September.

Table 1. Monthly extent linear trends, in % per decade relative to the 1981–2010 CDR climatology, for both hemispheres for the entire timeseries and for March and September. The difference trends are calculated from monthly differences between CDR and BT or NT. The 2 standard deviation range of the trend is given in parentheses below each trend value. Statistically significant trends ($p < 0.05$) are in *italics*.

Extent Trend	**Northern Hemisphere**			**Southern Hemisphere**		
(±2 SD)	**All**	**Mar**	**Sep**	**All**	**Mar**	**Sep**
CDR	***−5.04*** ***(1.93)***	***−2.84*** ***(0.43)***	***−13.7*** ***(2.02)***	−0.14 (3.51)	1.47 (3.43)	0.41 (0.57)
BT	***−4.71*** ***(1.90)***	***−2.65*** ***(0.44)***	***−13.9*** ***(2.20)***	−0.18 (3.48)	1.05 (3.34)	0.35 (0.58)
NT	***−4.48*** ***(1.93)***	***−2.50*** ***(0.43)***	***−12.7*** ***(1.99)***	0.13 (3.47)	1.65 (3.36)	0.50 (0.57)
CDR–BT	***−0.32*** ***(0.07)***	***−0.20*** ***(0.07)***	0.15 (0.44)	0.04 (0.05)	***0.42*** ***(0.20)***	*0.06* *(0.04)*
CDR–NT	***−0.56*** ***(0.05)***	***−0.35*** ***(0.07)***	***-0.98*** ***(0.21)***	***−0.27*** ***(0.06)***	***−0.18*** ***(0.22)***	***−0.09*** ***(0.07)***

However, because the overall trends have such small magnitudes in the Southern Hemisphere, the differences between the products have more of an impact. Most noticeable is that over the entire time series, NT yields a positive trend while CDR and BT have negative trends. All three trends are not statistically significant (at the $p < 0.05$ level) and because they are so close to zero, it is perhaps not surprising that the sign of the trend may be different. The reason may be the larger difference in NT extents during the SMMR period (Figure 3d). The March and September differences are all of the same sign (increasing trend), but none are statistically significant.

Now, examining the area trends, the general patterns are similar, but with an even larger difference between the NT estimates and the other two products (Figure 4). This results from the aforementioned concentration bias in the NT. That bias is visible in both hemispheres, but is particularly pronounced in the Southern Hemisphere, where differences in the maximum annual area are upwards of two million km^2. In contrast, the CDR-BT differences are much smaller. Similar to the extent results, there is a small but noticeable change in the differences across the SMMR to SSMI transition in 1987, particularly for CDR–BT. Again, this primarily reflects the difference between CDR and BT automated weather and land spillover filters.

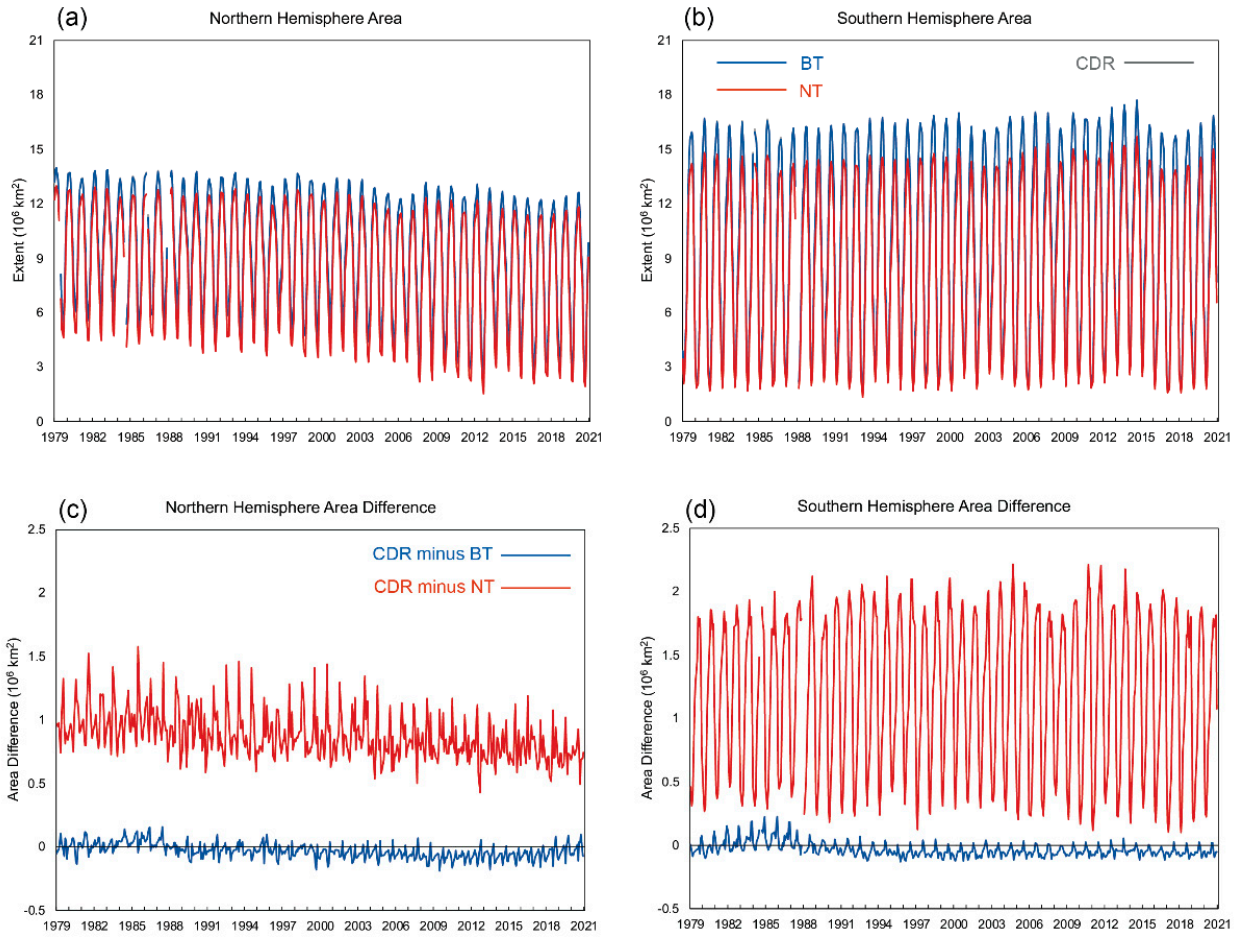

Figure 4. Total monthly sea ice area, 1979–2020 for (**a**) Northern Hemisphere and (**b**) Southern Hemisphere, and CDR–BT and CDR–NT area difference for (**c**) Northern Hemisphere and (**d**) Southern Hemisphere.

The area trends show similar differences as extent, with the Northern Hemisphere having statistically significant negative trends for all three products and all three time periods. The CDR and BT trends are more consistent with each other than with NT (Table 2). In particular, the magnitude of the September NT trend is substantially different,

2.88% per decade steeper than the CDR trend, whereas the BT and CDR September trends differ by only 0.1% per decade.

Table 2. Monthly area linear trends, in % per decade relative to the 1981–2010 CDR climatology, for both hemispheres for the entire timeseries and for March and September. The 2 standard deviation range of the trend is given in parentheses below each trend value. Statistically significant trends ($p < 0.05$) are in ***bold italics***.

Area Trend	**Northern Hemisphere**			**Southern Hemisphere**		
(±2 SD)	**All**	**Mar**	**Sep**	**All**	**Mar**	**Sep**
CDR	***−5.65*** ***(2.34)***	***−2.90*** ***(0.50)***	***−17.9*** ***(2.63)***	0.11 (3.82)	1.74 (3.85)	0.54 (0.66)
BT	***−5.40*** ***(2.34)***	***−2.71*** ***(0.50)***	***−17.8*** ***(2.76)***	0.31 (3.81)	1.85 (3.82)	0.69 (0.67)
NT	***−4.99*** ***(2.39)***	***−2.33*** ***(0.52)***	***−15.0*** ***(2.20)***	0.32 (3.38)	2.05 (3.43)	0.47 (0.65)
CDR–BT	***−0.26*** ***(0.04)***	***−0.19*** ***(0.05)***	−0.10 (0.29)	***−0.20*** ***(0.04)***	−0.10 (0.20)	***−0.15*** ***(0.06)***
CDR–NT	***−0.67*** ***(0.13)***	***−0.57*** ***(0.16)***	***−2.88*** ***(0.73)***	−0.21 (0.45)	−0.31 (0.66)	0.06 (0.21)

In the Southern Hemisphere, the area trends are slightly positive for all of the products and time periods, but none are statistically significant. The three products' area trends are reasonably consistent and unlike in the north, there is not a substantial discrepancy with the NT area trend during any of the three time periods.

3.3. Regional Extent and Area Trends

Next, we compared trends across the full time series, 1979 to 2020, in different regions of the Arctic and Antarctic. While regional trends from a given product have been calculated, e.g., [15,16] and hemispheric trends have been compared between products, e.g., [9], to our knowledge there has not been a regional comparison between products. Such a comparison can illuminate differing regional characteristics and may help assess the relative consistency across sensor transitions. As noted in [28], good agreement in hemisphere extents and areas may obscure offsetting differences regionally.

To conduct this comparison, we introduce a new set of regional masks. Regional masks were first developed for [29]. This was later expanded in [28], extending regions southward in the Northern Hemisphere and adding a Gulf of St. Lawrence region. These were further expanded in [30], which split the "Arctic Ocean" into a Central Arctic region and regions for coastal Arctic seas (Beaufort, Chukchi, East Siberian, and Laptev), as well as splitting the "Barents and Kara Seas" region into their individual seas. The boundaries of these splits were somewhat arbitrary, particularly the northern boundary of the coastal Arctic seas, created by manually drawn polygons.

The Antarctic regions were originally created for [31] and were based simply on longitudinal sectors; they have been unchanged other than a minor adjustment of the Weddell Sea region [15].

The regions were originally created on a 25 km polar stereographic grid. Thus, boundaries are specific to the 25 km resolution grid and the associated landmask. This presents limitations when regridding or reprojecting to a different grid or resolution. We note that a modified version of [30] is used for an operational product [32]. This modified version was produced by manually drawing vector polygons to closely approximate the polar stereographic gridded mask.

For this study, we implemented a new approach and created new regional masks (Figure 5). We referred to definitions from the International Hydrographic Organization (IHO) "Limits of Oceans and Seas" [33] as the starting point of the region definitions. However, we diverged from the definitions where such definitions were less suitable for

sea ice. For example, the IHO definition of the Beaufort Sea is a triangular region with a northern boundary extending from the southwest tip of St. Patrick's Island diagonally to Point Barrow. Such a small area does not capture the relevant ice dynamics at play in the region (e.g., the Beaufort Gyre). Instead, we extended the northern boundary westward from St. Patrick's Island along a line of constant latitude. We extended across the Chukchi and East Siberian Seas as well, enlarging those as well compared to the IHO definitions. We also considered consistency with the old masks when defining regions, such as providing a combined Baffin Bay/Davis Strait/Labrador Sea region.

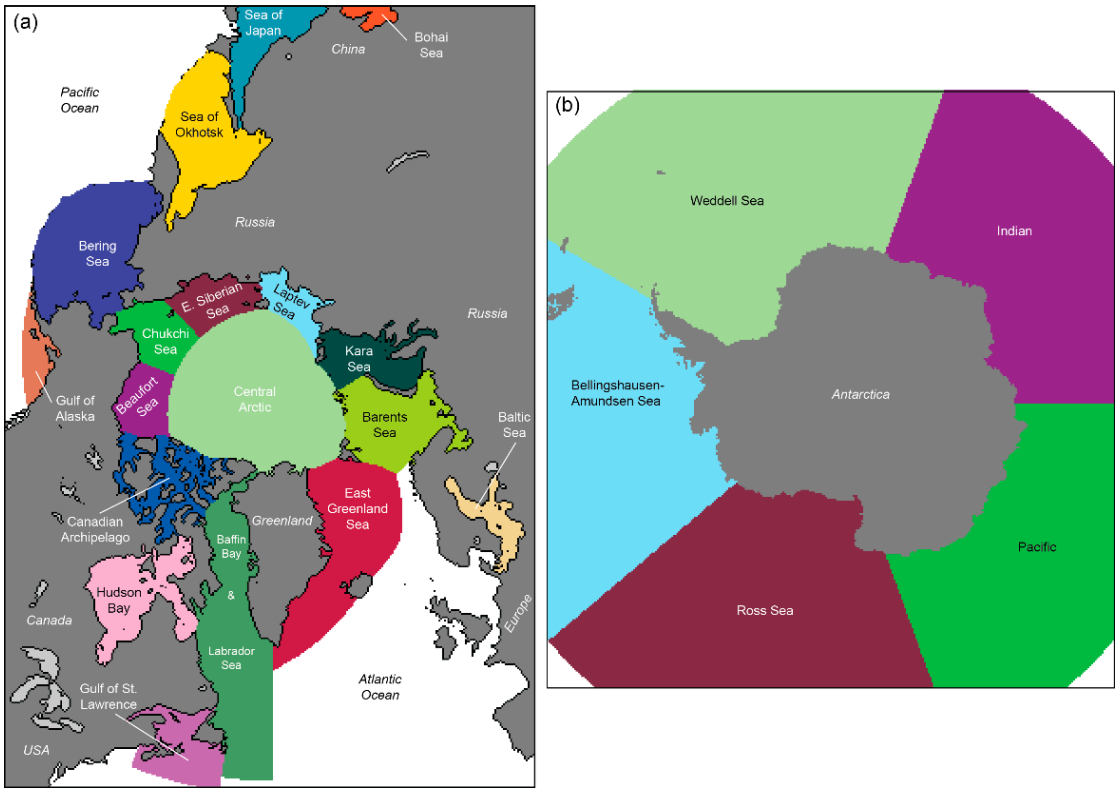

Figure 5. Map of (**a**) Northern Hemisphere and (**b**) Southern Hemisphere regions.

The regions were defined by manually describing vertices for the polygons within a GIS shapefile to enclose each region. The Southern Hemisphere region definitions are unchanged except that the longitudinal boundaries, bounded by −50°S south latitude, define vector polygons; small variations in the western Weddell and Ross Sea boundaries were made to not overlap ocean/sea ice areas (e.g., so that the Weddell extends to the Antarctic Peninsula at all latitudes). The polygons extend to overlap the land, which allows flexibility when reprojecting to different resolutions or projections and to account for possible differences in coastline from different databases. A GIS shapefile in latitude–longitude space is used as the baseline data source, which was then rasterized onto the 25 km polar stereographic grid for the analysis presented here. We note that a digitized version of the IHO definitions has been produced [34]. However, it bounds the regions with digitized shorelines. Because we desired flexibility for use with different coastline databases (and resolutions) and because we were making modifications to the boundaries, we chose not to use this source. In addition, the high-resolution coastline in [34] results in a large file that is unwieldy to work with.

We compare extent and area trends across the full time series. Some regions annually reach ice-free conditions during summer and some regions are fully ice-covered during winter. In such situations, there is no variability. Thus, computing the trend over all months through the time series will somewhat mute the trends and the differences between products. However, this approach provides a simple comparison that illuminates the

basic differences between the products. Trends for the Bohai Sea, Baltic Sea, and Gulf of Alaska were not included here because their small areas and limited ice cover do not yield useful trends.

The results show large variability in trends between regions. The variation reflects differences in the changes in the ice cover as well as the size of the individual regions. In the Northern Hemisphere (Figure 6), all of the trends are negative. The Barents Sea has the largest magnitude decreasing extent and area trend, while the Gulf of St. Lawrence has the smallest. All extent trends are statistically significant ($p < 0.05$). For area, all regions are statistically significant except Hudson Bay and the Bering Sea, which fall just short of the $p < 0.05$ criterion.

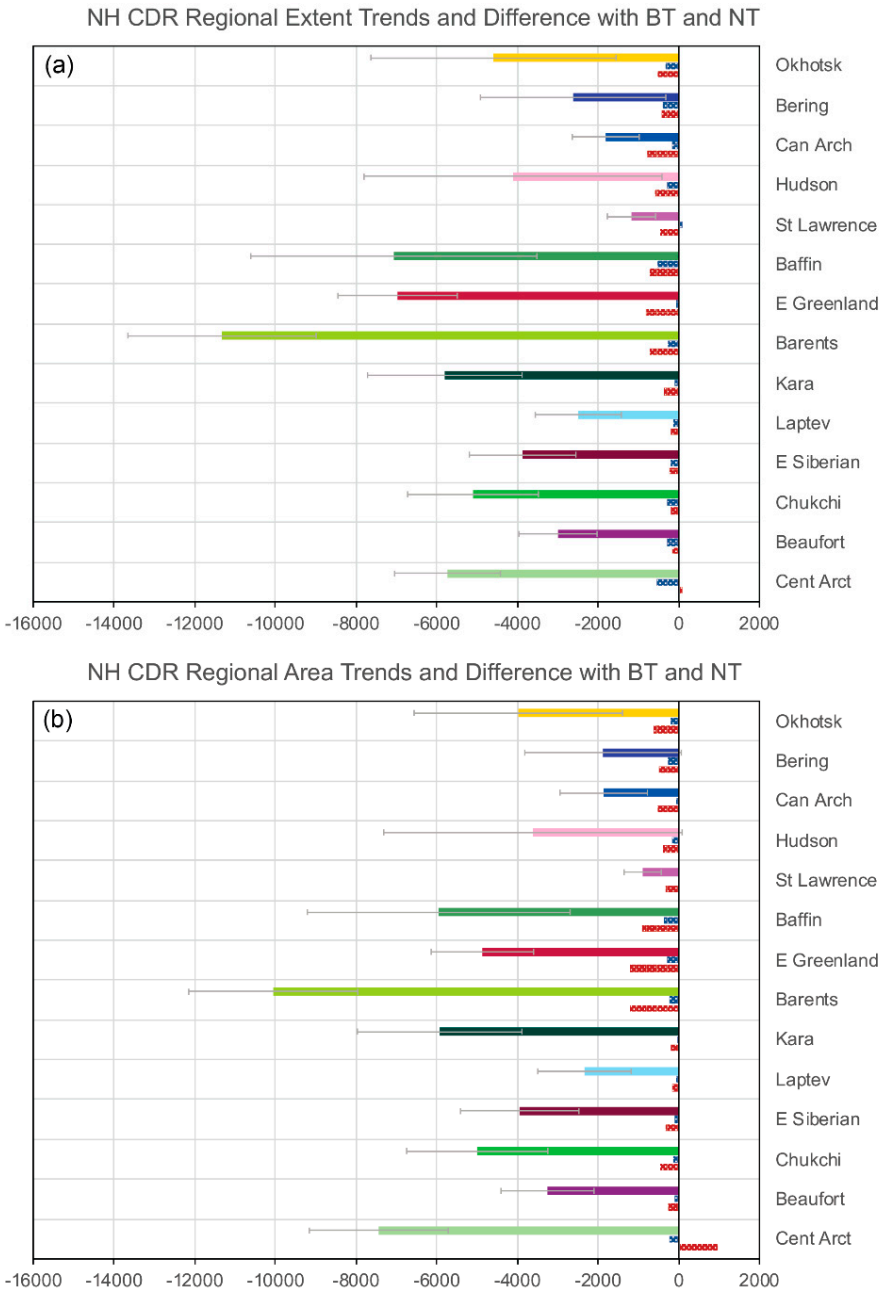

Figure 6. Northern Hemisphere regional (**a**) extent and (**b**) area trends in km^2 yr^{-1}. Solid color bars correspond to the region colors in Figure 5. The gray error bars represent the 2 standard deviation range of the linear trend fit. The blue hatched bar for each region indicates the CDR–BT trend and the red hatched bar indicates the CDR–NT trend.

The CDR–BT and CDR–NT trend differences are generally small compared to the overall trends, and as seen with the hemispheric trends, the BT trends are more consistent with CDR than are NT trends. The Northern Hemisphere difference trends are mostly negative, meaning that the CDR trends are less steep than BT or NT, i.e., the CDR extents and areas are decreasing more slowly than BT and NT. The notable exception is in the Central Arctic region where the CDR–NT trend is slightly positive for extent and substantially positive for area. This suggests that surface melt may be influencing the NT trend in this region.

The regional picture is substantially different in the Southern Hemisphere (Figure 7). First, only the Bellingshausen-Amundsen Sea region has negative extent and area trends; the other four regions have positive trends. Second, none of the trends are statistically significant. The second notable feature is that the extent difference trends for CDR–BT and CDR–NT are of the same magnitude as the extent trend values themselves. This reflects the fact that the extent trends are small overall, so even small differences between the products yield trend differences that are comparable to the extent trends. Another factor is that the Southern Hemisphere sea ice has a largely open boundary to north around the whole of the Antarctic continent. This means that even small biases in ice edge location between products sum up to relatively large differences in total extent, which can then influence the trend over the time series. This is supported by the very small trend differences in the CDR–BT and CDR–NT area (Figure 7b). Subsequently, the concentrations are reasonably consistent over time, and it is primarily low concentrations at the ice edge, which sit upon the razor's edge of the 15% concentration extent threshold, that cause notable differences in extent.

Overall, the Southern Hemisphere regional trends, like the hemispheric trends, indicate overall higher uncertainty in the extent and area trends because they are near zero and not statistically significant. Therefore, small differences in products are more noticeable and have a relatively larger effect.

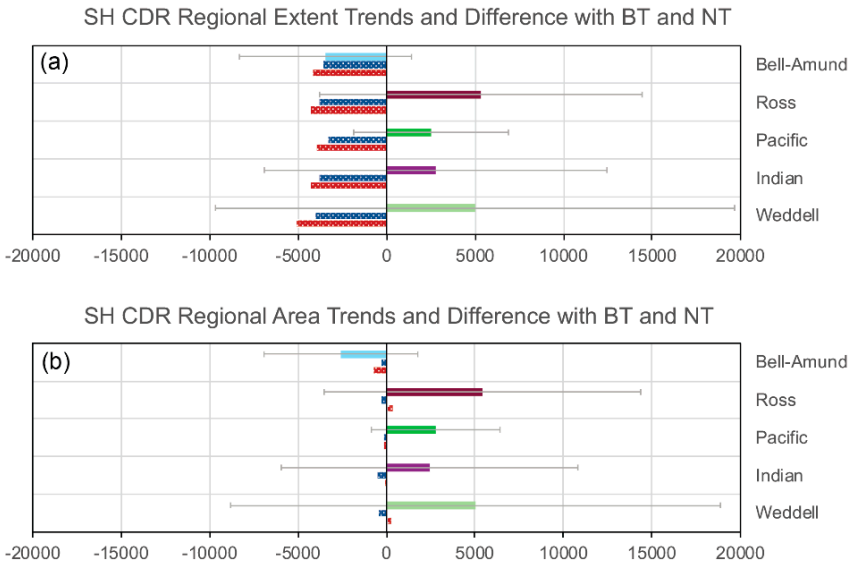

Figure 7. Southern Hemisphere regional (**a**) extent and (**b**) area trends in km^2 yr^{-1}. Solid color bars correspond to the region colors in Figure 5. The gray error bars represent the 2 standard deviation range of the linear trend fit. The blue hatched bar for each region indicates the CDR-BT trend and the red hatched bar indicates the CDR-NT trend.

4. Discussion

The main focus on this paper is to introduce the NOAA/NSIDC CDR Version 4 product and provide a comparison to the other two widely used passive microwave sea ice concentration products at NSIDC, based on the NASA Team and Bootstrap algorithms. The main advantage of the CDR over the NT and BT products is that it is fully automated, and

all processing is reproducible. In contrast, the NASA products employ manual corrections to remove erroneous weather effects, some land-spillover influence, and other errors in the data. This approach "cleans up" the products so that they have fewer artifacts, but at the cost of reproducibility. In the CDR product, some artifacts remain, particularly in the daily fields; these artifacts are ephemeral and thus tend to get averaged out in the monthly average fields. Such artifacts are most prominent in the SMMR period due to poorer quality T_B fields. Later data has many fewer issues, though weather effects and land-spillover still occur. As noted above, additional automated quality control procedures are implemented, namely applying both the NT and BT weather filters and land-spillover corrections. Additionally, for the SMMR component of the CDR, a daily valid-ice mask was created based on the maximum extent of the Goddard BT and NT fields (which include their manual corrections) during the SMMR. This difference in the CDR approach for SMMR explains the variation in the CDR–BT and CDR–NT values for 1979 to August 1987, which is particularly noticeable for extent (Figure 3), but also to a lesser degree for area (Figure 4).

Another factor in the differences between products is the manual corrections. Of particular note is the land-spillover issue. Even with the filters applied, some spillover error remains, resulting in false ice along the coast during ice-free conditions in some locations. Visual inspection of the products confirms that the BT product includes more aggressive removal of such spillover [35], resulting in "cleaner" coastlines compared to NT, as well as to the automated-only approach for CDR. Therefore, this is another source for BT and CDR differences.

These varying approaches to processing and quality control explain the month-to-month differences and seasonal differences. In addition, they also explain some of the differences in the trends. If different sensors have different characteristics, particularly SMMR, then such differences will influence long-term trends.

Another key factor for long-term trends is the inter-sensor calibration. To create a consistent time series, T_B fields are adjusted based on overlap periods where both the old and new sensors are both operating [16,28]. Typically, a regression of T_B values is carried out. Then, to further optimize the consistency, tie point values for pure surface types (100% ice and 100% water) are adjusted so that extent and/or area match as closely as possible. Sometimes, weather filter thresholds are also adjusted [26]. Both NT and BT have carried out these procedures completely independently using different domains (i.e., which T_B values are used within the T_B grids and what overlap time period is employed).

Typically, the T_B fields match well overall, but previous studies have shown that even small differences in T_B can result in notable differences in long-term trends, which can be particularly relevant in the Antarctic where trends are near zero and are borderline statistically significant [36]. There even appears to be a seasonal effect on inter-calibration—i.e., in which season an overlap occurs changes the derived match [37].

The CDR product uses the BT and NT processed concentrations as-is, including their varying inter-sensor calibrations. The differences in the CDR come from the automated quality control. Therefore, uncertainties in inter-sensor calibrations, as noted in [36], influence the CDR as well as the BT and NT estimates and their long-term trends. This confirms the conclusion in [36] that the "trend uncertainty"—i.e., the two standard deviation range of the trend and/or the statistical significance tests—does not fully encompass the overall uncertainty in the trend due to inter-sensor calibration, as well as differences in quality control measures.

A final observation, briefly mentioned above, is that the Northern Hemisphere NT area shows a fairly strong relative trend compared to the CDR (and BT) (Figure 4c), particularly for September. The CDR-NT trend is $-2.88 \pm 0.77\%$ per decade (Table 2), which means that the NT area is decreasing more slowly than the CDR area. However, notably, this trend is reversed in the Central Arctic, where the NT area trend is steeper (Figure 6b). This is likely related to increased surface melt in the region, which has been noted by several studies, e.g., [20]. The NT algorithm uses constant tie points for a given sensor—i.e., adjustments are only made at sensor transitions. In contrast, the BT algorithm uses varying tie points

that adjust daily. Because the CDR algorithm mostly uses BT output, the CDR values are also largely based on daily adjusted tie points. Changes in melt over time affect the T_B signature of the ice in the passive microwave data. The daily varying BT (and CDR) coefficients can adapt to the melt, but the constant NT tie points do not. Thus, in the Central Arctic, the increased melt is seen by NT as lower concentrations, imputing a melt-induced area trend. However, over the full hemisphere, the declining NT area trend is less steep than CDR, so there are other processes at play, likely related to the quality control measures and inter-sensor calibration. These warrant further study.

Overall, the CDR trends are reasonably consistent with BT and NT trends and effectively yield the same conclusions. Thus, the CDR provides a quality time series of sea ice concentration, extent, and area, that complements the BT and NT time series as well as other products, such as from OSI-SAF [4]. As numerous studies have shown, no passive microwave sea ice product is perfect, and all are limited by the spatial resolution of the sensors as well as factors affecting data quality such as weather and mixed land-ocean grid cells. As such, these products are not suitable for operational use. Nonetheless, the CDR and other algorithms provide useful long-term time series with which to assess climate change and variability.

Author Contributions: Conceptualization, W.N.M., J.S.S., A.W. and F.M.F.; methodology, W.N.M. and J.S.S.; software, J.S.S. and A.W.; formal analysis, W.N.M. and J.S.S.; investigation, W.N.M., J.S.S. and A.W.; data curation, A.W.; writing—original draft preparation, W.N.M.; writing—review and editing, W.N.M., A.W. and F.M.F.; visualization, W.N.M. and J.S.S.; supervision, F.M.F., A.W. and W.N.M.; project administration, F.M.F.; funding acquisition, F.M.F. and W.N.M. All authors have read and agreed to the published version of the manuscript.

Funding: This research was funded by the NOAA NCEI Climate Data Record Program through the NOAA Prime Contract #ST133017CQ0058, Task Order #1332KP19FNEEN0003, and the NASA Earth Science Data Information System (ESDIS) Project through the NASA Snow and Ice Distributed Active Archive Center (DAAC) at NSIDC, Grant #80GSFC18C0102.

Data Availability Statement: The gridded sea ice concentration fields from the NT, BT, and CDR algorithm products are available from NSIDC at cited references provided in the manuscript. Total extent and area statistics were calculated from the daily concentration fields (daily values averaged to obtain monthly values) and are available upon request.

Conflicts of Interest: The authors declare no conflict of interest.

References

1. Meier, W.N.; Perovich, D.; Farrell, S.; Haas, C.; Hendricks, S.; Petty, A.A.; Webster, M.; Divine, D.; Gerland, S.; Kaleschke, L.; et al. Sea ice. In *Arctic Report Card 2021*; Moon, T.A., Druckenmiller, M.L., Thoman, R.L., Eds.; NOAA, 2021. [CrossRef]
2. Parkinson, C.L.; DiGirolamo, N.E. Sea ice extents continue to set new records: Arctic, Antarctic, and global results. *Rem. Sens. Environ.* **2021**, *267*, 112753. [CrossRef]
3. Comiso, J.C.; Gersten, R.A.; Stock, L.V.; Turner, J.; Perez, G.J.; Cho, K. Positive Trend in the Antarctic Sea Ice Cover and Associated Changes in Surface Temperature. *J. Clim.* **2017**, *30*, 2251–2267. [CrossRef] [PubMed]
4. Lavergne, T.; Sørensen, A.M.; Kern, S.; Tonboe, R.; Notz, D.; Aaboe, S.; Bell, L.; Dybkjær, G.; Eastwood, S.; Gabarro, C.; et al. Version 2 of the EUMETSAT OSI SAF and ESA CCI sea-ice concentration climate data records. *Cryosphere* **2019**, *13*, 49–78. [CrossRef]
5. Ivanova, N.; Johannessen, O.M.; Pedersen, L.T.; Tonboe., R.T. Retrieval of Arctic sea ice parameters by satellite passive microwave sensors: A comparison of eleven sea ice concentration algorithms. *IEEE Trans. Geosci. Rem. Sens.* **2014**, *52*, 723–7246. [CrossRef]
6. Kern, S.; Lavergne, T.; Notz, D.; Pedersen, L.T.; Tonboe, R. Satellite passive microwave sea-ice concentration data set inter-comparison for Arctic summer conditions. *Cryosphere* **2020**, *14*, 2469–2493. [CrossRef]
7. Kern, S.; Lavergne, T.; Notz, D.; Pedersen, L.T.; Tonboe, R.T.; Saldo, R.; Sørensen, A.M. Satellite passive microwave sea-ice concentration data set intercomparison: Closed ice and ship-based observations. *Cryosphere* **2019**, *13*, 3261–3307. [CrossRef]
8. Kern, S.; Lavergne, T.; Pedersen, L.T.; Tonboe, R.T.; Bell, L.; Meyer, M.; Zeigermann, L.M. Satellite Passive Microwave Sea-Ice Concentration Data Set Inter-comparison using Landsat data. *Cryosphere* **2022**, *16*, 349–378. [CrossRef]
9. Comiso, J.C.; Meier, W.N.; Gersten, R. Variability and trends in the Arctic sea ice cover: Results from different techniques. *J. Geophys. Res.* **2017**, *122*, 6883–6900. [CrossRef]

10. Cavalieri, D.J.; Parkinson, C.L.; Gloersen, P.; Zwally, H.J. *Sea Ice Concentrations from Nimbus-7 SMMR and DMSP SSM/I-SSMIS Passive Microwave Data, Version 1*; NASA National Snow and Ice Data Center Distributed Active Archive Center: Boulder, CO, USA, 1996. [CrossRef]
11. Cavalieri, D.J.; Gloersen, P.; Campbell, W.J. Determination of sea ice parameters with the NIMBUS 7 SMMR. *J. Geophys. Res.* **1984**, *89*, 5355–5369. [CrossRef]
12. Fetterer, F.; Knowles, K.; Meier, W.N.; Savoie, M.; Windnagel, A. *Sea Ice Index, Version 3*; NSIDC National Snow and Ice Data Center: Boulder, CO, USA, 2017. [CrossRef]
13. Comiso, J.C. *Bootstrap Sea Ice Concentrations from Nimbus-7 SMMR and DMSP SSM/I-SSMIS, Version 3*; NASA National Snow and Ice Data Center Distributed Active Archive Center: Boulder, CO, USA, 2017. [CrossRef]
14. Comiso, J.C. Characteristics of Winter Sea Ice from Satellite Multispectral Microwave Observations. *J. Geophys. Res.* **1986**, *91*, 975–994. [CrossRef]
15. Parkinson, C.L.; Cavalieri, D.J.; Gloersen, P.; Zwally, H.J.; Comiso, J.C. Arctic sea ice extents, areas, and trends, 1978–1996. *J. Geophys. Res.* **1999**, *104*, 20837–20856. [CrossRef]
16. Comiso, J.C.; Nishio, F. Trends in the Sea Ice Cover Using Enhanced and Compatible AMSR-E, SSM/I, and SMMR Data. *J. Geophys. Res.* **2008**, *113*, C02S07. [CrossRef]
17. Meier, W.N.; Fetterer, F.; Windnagel, A.K.; Stewart, J.S. *NOAA/NSIDC Climate Data Record of Passive Microwave Sea Ice Concentration, Version 4*; NSIDC National Snow and Ice Data Center: Boulder, CO, USA, 2021. [CrossRef]
18. Comiso, J.C.; Cavalieri, D.J.; Parkinson, C.L.; Gloersen, P. Passive microwave algorithms for sea ice concentration: A comparison of two techniques. *Rem. Sens. Environ.* **1997**, *60*, 357–384. [CrossRef]
19. Barber, D.; Meier, W.N.; Gerland, S.; Mundy, C.J.; Holland, M.; Kern, S.; Li, Z.; Michel, C.; Perovich, D.K.; Tamura, T. Arctic Sea Ice. In *Snow, Water, Ice, and Permafrost in the Arctic (SWIPA) 2017*; Arctic Monitoring and Assessment Programme (AMAP): Oslo, Norway, 2017; pp. 104–136.
20. Bliss, A.C.; Anderson, M.R. Arctic sea ice melt onset timing from passive microwave-based and surface air temperature-based methods. *J. Geophys. Res.* **2018**, *123*, 9063–9080. [CrossRef]
21. Windnagel, A.; Sea Ice Concentration Climate Algorithm Theoretical Basis Document (C-ATBD) Climate Data Record Program. CDRP-ATBD-0107, Revision 9. Available online: https://nsidc.org/sites/nsidc.org/files/technical-references/CDRP-ATBD-final.pdf (accessed on 3 June 2021).
22. Gloersen, P. *Nimbus-7 SMMR Polar Gridded Radiances and Sea Ice Concentrations, Version 1*; NASA National Snow and Ice Data Center Distributed Active Archive Center: Boulder, CO, USA, 2006. [CrossRef]
23. Windnagel, A.; Meier, W.; Stewart, S.; Fetterer, F.; Stafford, T. NOAA/NSIDC Climate Data Record of Passive Microwave Sea Ice Concentration Version 4 Analysis. In *NSIDC Special Report 20*; National Snow and Ice Data Center: Boulder, CO, USA, 2021. Available online: https://nsidc.org/sites/nsidc.org/files/technical-references/NSIDC-Special-Report-20.pdf (accessed on 20 December 2021).
24. Meier, W.N.; Stewart, J.S. Assessing uncertainties in sea ice extent climate indicators. *Environ. Res. Lett.* **2019**, *14*, 035005. [CrossRef]
25. Cavalieri, D.J.; Germain, K.M.S.; Swift, C.T. Reduction of weather effects in the calculation of sea ice concentration with the DMSP SSM/I. *J. Glaciol.* **1995**, *41*, 455–464. [CrossRef]
26. Cavalieri, D.J.; Parkinson, C.L.; Di Girolamo, N.; Ivanov, A. Intersensor calibration between F13 SSMI and F17 SSMIS for global sea ice data records. *IEEE Geosci. Rem. Sens. Lett.* **2012**, *9*, 233–236. [CrossRef]
27. Parkinson, C.L.; (NASA Goddard Space Flight Center, Greenbelt, MD, USA). Personal communication, 2016.
28. Cavalieri, D.J.; Parkinson, C.L.; Gloersen, P.; Comiso, J.C.; Zwally, H.J. Deriving Long-term Time Series of Sea Ice Cover from Satellite Passive-Microwave Multisensor Data Sets. *J. Geophys. Res.* **1999**, *104*, 15803–15814. [CrossRef]
29. Parkinson, C.L.; Comiso, J.C.; Zwally, H.J.; Cavalieri, D.J.; Gloersen, P.; Campbell, W.J. *Arctic Sea Ice, 1973–1976: Satellite Passive-Microwave Observations*; NASA SP-489; National Aeronautics and Space Administration: Washington, DC, USA, 1987; p. 296.
30. Meier, W.N.; Stroeve, J.; Fetterer, F. Whither Arctic sea ice? A clear signal of decline regionally, seasonally and extending beyond the satellite record. *Ann. Glaciol.* **2007**, *46*, 428–434. [CrossRef]
31. Zwally, H.J.; Comiso, J.C.; Parkinson, C.L.; Campbell, W.J.; Carsey, F.D.; Gloersen, P. *Antarctic Sea Ice, 1973–1976: Satellite Passive-Microwave Observations*; NASA SP-459; National Aeronautics and Space Administration: Washington, DC, USA, 1983; p. 206.
32. U.S National Ice Center and National Snow and Ice Data Center. *Multisensor Analyzed Sea Ice Extent—Northern Hemisphere (MASIE-NH), Version 1*; Fetterer, F., Savoie, M., Helfrich, S., Clemente-Colón, P., Eds.; National Snow and Ice Data Center (NSIDC): Boulder, CO, USA, 2010. [CrossRef]
33. IHO. *International Hydrographic Organization Limits of Oceans and Seas*, 3rd ed.; Special Publication No. 23; International Hydrographic Organization: Monte Carlo, Monaco, 1953. Available online: https://epic.awi.de/id/eprint/29772/1/IHO1953a.pdf (accessed on 10 February 2021).
34. Fourcy, D.; Lorvelec, O. A new digital map of limits of oceans and seas consistent with high-resolution global shorelines. *J. Coast. Res.* **2013**, *29*, 471–477. [CrossRef]

35. Comiso, J.C.; (NASA Goddard Space Flight Center, Greenbelt, MD, USA). Personal communication, 2016.
36. Eisenman, I.; Meier, W.N.; Norris, J.R. A spurious jump in the satellite record: Has Antarctic sea ice expansion been overestimated? *Cryosphere* **2014**, *8*, 1289–1296. [CrossRef]
37. Meier, W.N.; Khalsa, S.J.S.; Savoie, M.H. Intersensor calibration between F-13 SSM/I and F-17 SSMIS near-real-time sea ice estimates. *IEEE Trans Geosci. Rem. Sens.* **2011**, *49*, 3343–3349. [CrossRef]